Korean J. Chem. Eng., 34(10), 2619-2630 (2017)
DOI: 10.1007/s11814-017-0162-6

pISSN: 0256-1115
eISSN: 1975-7220

Pb(II) ion adsorption by biomass-based carbonaceous fiber modified by the integrated oxidation and vulcanization

Xiaoxiang Jiang* and Dekui Shen,†**

*Engineering Laboratory of Energy System Process Conversion & Emission Control Technology of Jiangsu Province, School of Energy and Mechanical Engineering, Nanjing Normal University, Nanjing 210042, P. R. China
**Key Laboratory of Energy Thermal Conversion and Control of Ministry of Education, Southeast University, Nanjing 210096, P. R. China
(*Received 16 May 2016 • accepted 12 June 2017*)

Abstract−Biomass-based activated carbonaceous fiber (ACF) was modified by nitric-acid oxidation under microwave heating (ACF-O) and then further treated by thioglycolic acid (ACF-S) to prepare carbon materials with high capability for the removal of Pb(II) ions. The physico-chemical properties of the original and modified ACF samples were characterized by X-ray diffraction (XRD), Fourier transform infrared spectroscopy (FT-IR), Zeta potential, Boehm titration, BET, Raman spectrum and X-ray photoelectron spectroscopy (XPS). It was found that modification treatments damage the pore and graphite crystalline structure of ACF, while the micropore structure is protected and extra oxygen-containing surface functional groups are grafted on its surface. The adsorption performance of the original and the modified ACF samples affected by adsorption conditions regarding to Pb(II) ion strength (10 mg/L-105 mg/L), contact time (10 min-120 min), pH value (2.5-6.5), and solvent temperature (15 °C-45 °C) was investigated through batch experiments. Compared to the maximum Pb(II) ion adsorption capacity of 75.24 mg/g by ACF sample, the value was substantially improved by the integrated modification method (193.42 mg/g for ACF-O and 209.21 mg/g for ACF-S sample). The *Biot* number determined from the homogeneous surface diffusion model (HSDM) was between 1 and 100 for the original and modified ACF samples, suggesting that the adsorption process of Pb(II) ions is limited by both the surface diffusion and film mass transfer.

Keywords: Activated Carbonaceous Fiber, Modification, Adsorption, Pb(II) Ions, Isotherms, Kinetics

INTRODUCTION

With rapid economic development, a large amount of wastewater containing Pb(II) ions is evolved from battery manufacturing, basic steel, paper and pulp, metal plating, leather tanning, agrochemicals, petrochemicals and fertilizer industries. Lead is stable in the environment but hazardous at high concentrations in the form of ion state, likely resulting in damage to the human neuronal system [1]. It is necessary to control the concentration of Pb(II) ions in natural water system by means of high-efficiency removal of the Pb(II) from different effluents.

Activated carbonaceous fiber (ACF) is widely used to remove various pollutants from water system [2], such as phenols [3], methylene blue [4], pesticides [5], dyes [6] Cu^{2+} [7], Pb^{2+} [8], Cr(VI) and p-nitrophenol [9], due to its outstanding morphological characteristics and adsorption performance. A number of modification methodologies were developed to improve the absorption characteristics of ACF (such as the adsorption capacity, selectivity and hydrophilicity) [10,11]. Chemical modification, which normally employed a certain amount of solvent to treat the activated carbonaceous materials to rearrange the pore size distribution and the surface functional groups, is considered one of the most fast and effective methods [12-18]. For example, nitric acid oxidation modification was found to be effective to enlarge the distribution of surface oxygen-containing functional groups [19-21]. The efficiency of nitric-acid oxidation modification was further enhanced as it was assisted by microwave heating [22]. The improvement on surface functional groups after nitric-acid oxidation and nitric-acid oxidation assisted with microwave heating was mainly related to oxygen- or nitrogen-containing functional groups. There are also studies that indicated thiol-function groups on the surface of carbonaceous absorbents also perform the integrated adsorption capability for different heavy metal ions [23,24]. Accordingly, it is interesting to develop some effective modification technologies on adsorption capacity of carbonaceous materials.

In present study, the activated carbonaceous fiber (ACF) prepared from sisal fiber was modified by microwave nitric-acid oxidation under microwave heating to produce ACF-O sample. ACF-O sample was then treated by thioglycolic acid to produce ACF-S for investigating the joint function of the two modification technologies (nitric-acid oxidation and thioglycolic-acid vulcanization). The prepared ACF, ACF-O and ACF-S samples were characterized by XRD, FT-IR, Zeta potential, Boehm titration, BET, Raman spectrum and XPS, while the adsorption capacity of Pb(II) ions from aqueous system was estimated through the batch adsorption experiments regarding the variation of contact time, solvent pH value and

†To whom correspondence should be addressed.
E-mail: 101011398@seu.edu.cn

solvent temperature. The isothermal performance for the adsorption of Pb(II) ions by the original and modified ACF samples was analyzed, and a homogeneous surface diffusion model (HSDM) was adopted to describe the kinetic process for Pb(II) ions adsorption by the original and modified ACF samples.

EXPERIMENTAL

1. Reagents and Chemicals

The solution of Pb(II) was prepared by dissolving lead nitrate ($Pb(NO_3)_2$) (GR grade) in deionized water and handled with analytical micropipettes. The pH value of solution was adjusted by 0.1 mol/L of sulfuric acid or 0.1 mol/L sodium hydroxide.

2. The Preparation of Sisal-based Activated Carbonaceous Fiber (ACF)

The sisal fiber was washed with the deionized water and then dried in an oven at 80 °C for 24 h. Before being sealed, the sisal fiber was impregnated by zinc chloride solution (mass fraction of 10%) with the mass ratio of 1 : 1.25. The mixture was sealed in a glass container at 80 °C for 12 h and then dried at 105 °C. The impregnated sisal fiber was then pre-oxidized at 250 °C for 60 min, followed by the activation process in continuous nitrogen flow (200 mL/min) at 600 °C for 50 min in an electric and microwave hybrid heating tubular furnace with the heating rate of 10 °C/min. The product of sisal-based activated carbonaceous fiber (ACF) was washed by 0.1 mol/L HCl and then by deionized water until the effluent solution pH remained constant.

3. Modification of the Prepared ACF by Oxidation and Vulcanization

3-1. Nitric-acid Oxidation of ACF Sample

0.07 g ACF and 35 mL nitric acid solution were mixed in a specimen cup and then placed in microwave-reactor instrument (MDS-6 manufactured by Xinyi Microwave Chemical Technology Co., Ltd.) under the fixed condition: nitric acid concentration (6.5-11.0 mol/L), modification temperature (90-150 °C), reaction time (5-20 min) and microwave power (400-1,000 W). The modified ACF sample was washed by deionized water until the solution pH remained constant and then dried. The ACF sample modified by nitric-acid oxidation under microwave heating was abbreviated as ACF-O.

To determine the optimum conditions and estimate the significant order of the experimental factors on the nitric-acid oxidation modification process, an orthogonal array of experiments of $L_{16}(4^5)$ matrix was designed, including the concentration of nitric acid (factor A), modification temperature (factor B), modification time (factor C) and microwave power (factor D) [25].

The result of Pb(II) ions adsorption capacity by the ACF-O sample under the different modification conditions varied from 83.09 to 97.03 mg/g (Table 1), giving the range analysis and ANOVA in Table 2 and Table 3. The vacant column is to evaluate the possible error of the experiments, while the range value (R_i) reflects the significance of the factors on Pb(II) absorption capacity for the ACF-O. Therefore, the significant order of factors can be estimated as factor B>factor D>factor A>factor C. The highest adsorption capacity of Pb(II) ions for the factors of each level was determined as: concentration of nitric acid 9.5 mol/L, modification temperature 150 °C, modification time 15 min, and microwave power 800 W.

Table 1. Results of the orthogonal array experiments

Number	Factor				Error	Adsorption capacity (mg/L)
	A (mol/L)	B (°C)	C (min)	D (w)		
1	6.5	130	5	400	1	83.09
2	6.5	140	10	600	2	89.44
3	6.5	150	15	800	3	96.81
4	6.5	160	20	1000	4	91.45
5	8	130	10	800	4	88.84
6	8	140	5	1000	3	91.09
7	8	150	20	400	2	96.67
8	8	160	15	600	1	94.73
9	9.5	130	15	1000	2	88.17
10	9.5	140	20	800	1	94.77
11	9.5	150	5	600	4	97.03
12	9.5	160	10	400	3	92.52
13	11	130	20	600	3	87.06
14	11	140	15	400	4	90.25
15	11	150	10	1000	1	93.35
16	11	160	5	800	2	91.89

Table 2. Range analysis of adsorption capacity from the orthogonal array experiments

Value name	A	B	C	D
K_1	360.79	347.15	363.09	362.52
K_2	371.33	365.54	364.15	368.26
K_3	372.48	383.87	369.96	372.31
K_4	362.54	370.59	369.94	364.06
k_1	90.2	86.79	90.77	90.63
k_2	92.83	91.38	91.04	92.06
k_3	93.12	95.97	92.49	93.08
k_4	90.64	92.65	92.49	91.01
R_i	360.79	9.18	1.72	2.45

Table 3. ANOVA analysis for adsorption capacity from the orthogonal array experiments

Factor	SS	DOF	MS	F	Type of effect
A	26.74	3	8.91	48.65	Significant
B	173.28	3	57.76	315.33	Highly significant
C	10.15	3	3.38	18.47	Significant
D	14.57	3	4.86	26.51	Significant
Error	0.55	3	0.18		

Critical value: $F_{0.05}(3,3)=9.25$ and $F_{0.01}(3,3)=29.5$

And compared to the other factors, modification temperature was estimated to the most significant one for the microwave nitric-acid oxidation process of ACF sample [26].

3-2. Thioglycolic-acid Vulcanization of ACF-O Sample

2 g of ACF-O sample was placed in a conical flask with 12 mL thionyl chloride. The flask was sealed with a plastic film and then placed in an ice-bath for 1.5 h. The redundant thionyl chloride in

flask was removed by small-bore straw and followed by adding 14 mL thioglycolic acid for 2 h at 25 °C. The treated solid in the flask was filtered, washed with deionized water for several times and then dried for 10 h at 50 °C. The obtained solid product through the thioglycolic-acid vulcanization process is abbreviated as ACF-S in this work.

4. Characterization of the Original and Modified ACF Samples

4-1. XRD Analysis

X-ray diffraction (XRD) patterns were recorded using Smartlab XRD-3 with Cu Kα radiation to determine the crystal structure and phase of adsorbents. Scanning angle was conducted at 10-90 °C and the power used was 3 kW.

4-2. FT-IR Analysis

Functional group distribution of the ACF-O and ACF-S samples was characterized by Fourier transform infrared spectroscopy (FT-IR, Bruker Vector 22). Powdered KBr was mixed, grinded with 1% sample and then pressed into a disc for analysis with the spectrum scanned from 4,000 to 400 cm^{-1}.

4-3. Zeta Potential

Zeta potential represents the net external charge on the shearing surface of absorbents [27]. Carbon-based materials are normally amphoteric stuff because of the dissociation of surface functional groups or the existence of the π electron system due to the produced Lewis basic [28]. The zeta potential (pH_{IEP}) of the ACF, ACF-O and ACF-S was determined by Zetasizer Nano. A fixed amount of the sample was placed in deionized water, configuring the original and modified ACF samples suspension liquid of different pH values for Zeta potential measurement. The zero potential point of the sample was calculated by the interpolation method.

4-4. Boehm Titration

The quantity of surface oxygen-containing functional groups was determined by Boehm titration. 0.5 g of the sample was added in 50 ml of 0.1 mol/L solution of sodium hydroxide, sodium carbonate and sodium bicarbonate separately. The mixture was stirred in a closed vessel for 48 h. The suspension was then filtered, and the filtrate was titrated by hydrochloric acid of 0.05 mol/L by using an auto-titration system (ZDJ-5).

4-5. BET Analysis

The pore characteristics of the original and modified ACF samples were determined by the specific surface area and pore analyzer (ASAP 2020 M). Before N_2-adsorption at 77 K, the ACF sample was heated to 300 °C and degassed for 120 min under vacuum condition [29,30] while the ACF-O and ACF-S were heated to 100 °C for degassing for 360 min. The total specific surface area and microporous specific surface area were calculated through the BET method and t-plot equation [22].

4-6. Raman Analysis

The Raman spectra of graphite crystals result from the vibration or rotational energy of lattice and can represent the degree of structural order [31]. Raman analysis was conducted by means of RAM-PRO-785E (Agiltron US) spectroscopy. The laser power and wavelength at the sample surface was controlled at about 10 mW and 785 nm, respectively. During the measurement, the sample was dispersed in the deionized water.

4-7. XPS Analysis

X-ray photoelectron spectroscopy (XPS) analysis identifies the distribution of elemental composition in forms of functional groups on the surface of absorbents [32,33]. XPS analysis was performed by using an ESCALAB 250Xi analyzer with Al Kα X-ray source. The energy range was below 500 eV.

5. Batch Experiments for Heavy Metal Ions Absorption

Adsorption experiments for Pb(II) ions by the original and modified ACF samples were in a temperature-controlled water bath shaker with a stirring rate of 180 rpm. The effects of contact time (0-120 min), initial pH value (2.5-6.5) and solvent temperature (15-45) on the adsorption performance were investigated. The species of Pb(II) ions at different pH values was estimated by the Visual MINTEQ software [34-36].

100 mL lead nitrate solution with certain concentration was added in a set of 150 mL conical flasks. Sodium hydroxide and sulfuric acid were used to adjust the pH value of solution. A certain amount of the original or modified ACF sample was placed in the conical flasks for the removal of Pb(II) ions under the fixed condition. After that, the solution was filtered and the filtrate was analyzed by ICP (Inductive coupled plasma emission spectrometer) to determine the concentration of Pb(II) ions at the equilibrium state of adsorption.

6. Thermodynamic Analysis for Pb(II) Ions Adsorption Process

Thermodynamic parameters such as Gibbs free energy (ΔG), enthalpy (ΔH) and entropy (ΔS) of Pb(II) ions adsorption process can be evaluated from Eqs. (1)-(4):

$$K_c = \frac{C_0 - C_e}{C_e} \tag{1}$$

$$\Delta G = -RT\ln k_c \tag{2}$$

$$\Delta G = \Delta H - T\Delta S \tag{3}$$

Then:

$$\ln k_c = -\frac{\Delta H}{RT} + \frac{\Delta S}{R} \tag{4}$$

where, k_c is equilibrium constant. R is the molar gas constant, 8.314 J/(mol·K). ΔG is Gibbs free energy for the adsorption process, J/mol. The value of ΔH distinguishes the physical adsorption or chemical adsorption due to larger number of enthalpy of chemical adsorption, kJ/mol [37,38].

7. Adsorption Isothermal Models

The Langmuir isotherm is widely used to analyze the homogeneous, monolayer and ideal adsorption process. The Langmuir equation is expressed as:

$$\frac{q_e}{q_0} = \frac{bC_e}{1 + bC_e} \tag{5}$$

where q_0 is the Langmuir monolayer maximum adsorption capacity, mg/g; b is Langmuir adsorption intensity constant, related to the heat of adsorption, which can reflect solid surface affinity and the stability of bond between adsorbate and adsorbent, L/g [39,40].

The Freundlich isotherm adsorption equation is semi-empirical with the assumption of the adsorption process on the heterogeneous surface [41-43].

The Freundlich model is described as follows:

$$q_e = k_q C_e^{1/n} \tag{6}$$

where k_q is Freundlich isotherm constant about adsorption capacity, mg/g, n is a constant, reflecting the degree of difficulty for the adsorption process. When 2<n<10, adsorption proceeds easily, but is difficult when n<0.5.

RESULTS AND DISCUSSION

1. Characterization of Absorbents

1-1. XRD Analysis

XRD was used to analyze the crystalline structure of ACF, ACF-O and ACF-S samples (Fig. 1(a)). The peak around 24° is assigned to the (002) diffraction surface, while the peak around 43° is ascribed to the (100) diffraction surface [44]. The two diffraction peaks around 24° and 43° reflecting the turbostratic graphite structure are all observed for the three samples. The intensity of the two peaks becomes weak and the band of 2θ=43° shifts to the small diffraction angle after oxidation modification (ACF-O). This indicates that the interlamellar space is increased and the graphite crystallite size declines for the ACF-O sample, leading to the improvement of the adsorption capacity due to the increase of unsaturated carbon atom number on edges of the sample. Similar phenomenon can be observed for the XRD profile of ACF-S sample, confirming the destruction of the graphite crystalline structure by the two modification methods [45].

1-2. Surface Chemistry Characteristics of ACF, ACF-O and ACF-S Samples

FT-IR spectra of the ACF, ACF-O and ACF-S samples are shown in Fig. 1(b). For the ACF sample, the strong broad absorption band around 3,400 cm^{-1} is ascribed to the hydroxyl (-OH) stretching vibration. The band about at 1,510-1,600 cm^{-1} corresponds to the stretching vibration of the carbonyl (C=O) groups and C=C groups. The peak at 1,448 cm^{-1} is assigned to C-H or C=C groups. The absorption band in the region around 1,100 cm^{-1} probably represents the asymmetric vibration peak of ether bond or C-N.

Absorbance intensity of almost all characterized bands of ACF-O sample is larger than that of ACF sample. New absorbance peaks are observed in FITR spectrum of ACF-O sample, probably due to the oxidization reactions by nitric acid in the modification process. For example, the he absorbance peak around 1,700 cm^{-1} is attributed to the carbonyl (C=O) groups by ketone, carboxyl or ester. The band between 1,540 cm^{-1} and 1,353 cm^{-1} can be ascribed to the asymmetric stretching vibration of nitro (-NO_2) [46], while the peak at 1,253 cm^{-1} corresponds to the bending vibration of C-O. The absorbance intensity of the peak at 3,400 cm^{-1} is notably decreased for ACF-S sample, suggesting that -OH group on ACF-O sample might be removed and substituted by thioglycolic-acid

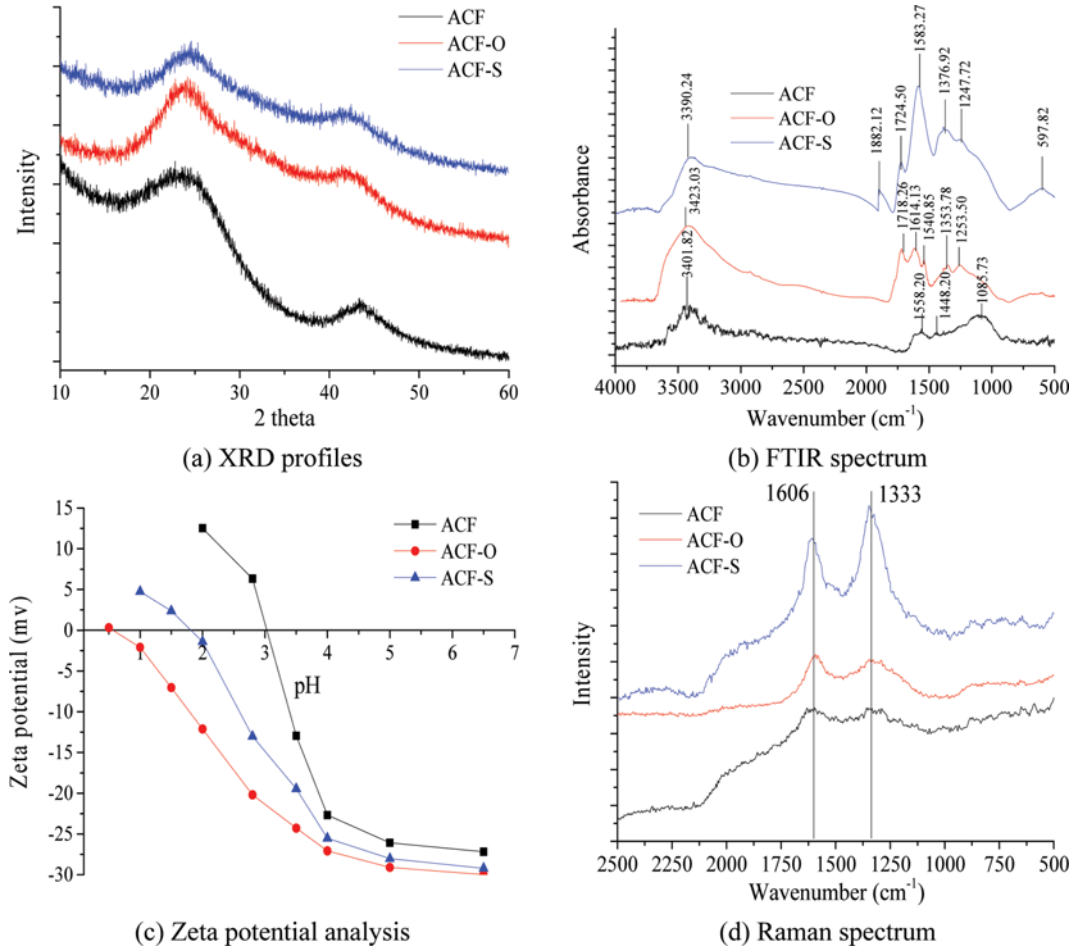

Fig. 1. Characterization for ACF, ACF-O and ACF-S samples.

Table 4. Boehm titration result for the ACF, ACT-O and ACF-S samples

Characterization	Parameters	ACF	ACF-O	ACF-S
Boehm titration	Carboxyl (mmol/g)	0.31	1.93	1.21
	Ester (mmol/g)	0.097	0.41	1.28
	Phenolic hydroxyl (mmol/g)	1.76	3.58	2.25
	Surface acidity (mmol/g)	2.17	5.92	4.74

through esterification reaction. The bands around 1,882 cm^{-1} and 1,600 cm^{-1} ascribed to the stretching vibration of C=O are intensified. This indicates that the surface oxygen-containing functional group of ACF sample is significantly modified through the nitric-acid oxidation and thioglycolic-acid vulcanization.

The content of carboxyl, ester and phenolic hydroxyl groups of ACF sample determined by analysis of Boehm titration is significantly increased after the two modification processes (Table 4). The content of ester group in ACF-S sample is larger than that of ACF-O sample, while the content of both carboxyl and phenolic hydroxyl group is smaller than that of ACF-O sample, confirming the finding in the FT-IR analysis of the three samples. Functional groups such carboxyl and hydroxyl in carbonaceous absorbents can help promote the adsorption of Pb(II) ions through the enhanced chemical adsorption [47].

The Zeta potential of the ACF, ACF-O and ACF-S samples is shown in Fig. 1(c). The pH_{IEP} of ACF-O is declined from 3.02 to 0.56 after the oxidation modification, probably attributed to the increment of the surface acidic groups such as carboxylic and phenolic hydroxyl groups [48]. Through the thioglycolic-acid vulcanization of ACF-O sample, the pH_{IEP} of ACF-S sample is increased to 1.82. The smaller Zeta potential of the carbonaceous adsorbent gives rise to the stronger electronegativity, better adsorption capacity of Pb(II) ions and more stable performance in the solution.

1-3. Pore Structure Characteristics

The key pore characteristics of the ACF, ACF-O and ACF-S samples are shown in Table 5 including surface area, pore volume and mean pore size. After the modification of ACF, the total surface area and pore volume is notably decreased from 2,055.53 m^2/g and 1.04 cm^3/g to 590.27 m^2/g and 0.29 cm^3/g for ACF-O and 440.72 m^2/g and 0.26 cm^3/g for ACF-S. However, the ratio of micropore surface area to the total surface area is 65.99% for ACF-O and 47.78% for ACF-S, compared to that of 35.55% for the original ACF sample. The two modification processes lead to the significant damage of the porous structure of the original ACF sample, but protect the micropores to a different extent.

1-4. Raman Spectrum Analysis

The Raman spectra of graphite crystals result from the vibration or rotational energy of lattice and can represent the degree of structural order [31]. The Raman spectrum of ACF, ACF-O and ACF-S samples is shown in Fig. 1(d) and Fig. 1S. All three samples exhibit two significant absorbance bands: 1) The G band around 1,580 cm^{-1} corresponding to the ideal graphitic lattice by the stretching of sp^2 atomic pairs on carbon ring; 2) The D band with the peak at 1333 is composed of a set of D_1, D_2, D_3 and D_4, reflecting the disorder or defection of crystal structure of the carbonaceous sample [49]. The D_1 band around 1,360 cm^{-1} is ascribed to the crystal lattice vibration mode with A1g symmetry reflecting the disorder of graphitic lattice; the D_2 around 1,620 cm^{-1} corresponds to the E_{2g} mode for the graphite layers; the D_3 around 1,500 cm^{-1} corresponds to amorphous carbon, and D_4 around 1,180 cm^{-1} corresponds to the disordered crystal or ionic impurities (where A represents single degenerate state of axis symmetry and E represents double degenerate state).

The two significant peaks around 1,606 cm^{-1} and 1,333 cm^{-1} are observed for all three samples. The $J_t=M_D/M_G$ values for the ACF-O and ACF-S are larger than that of ACF (Table 6 and Fig. 1S). And the J_3 and J_4 for ACF-S are much larger than those of ACF and ACF-O, confirming that the graphite crystallite size of ACF is greatly decreased after the oxidation and sequent vulcani-

Table 5. Pore structure characteristics of the ACF, ACF-O and ACF-S samples

Adsorbents	Surface area (m^2/g)				Pore volume (cm^3/g)			Mean pore size (nm)
	A_{bet}	A_{micro}	A_{mseo}	A_{micro}/A_{bet}	V_{micro}	V_{meso}	V_{total}	$\overline{D}$
ACF	2055.53	730.66	729.89	0.3555	0.31	0.47	1.04	2.02
ACF-O	590.27	389.54	117.21	0.6599	0.15	0.10	0.29	1.96
ACF-S	440.72	210.57	90.95	0.4778	0.094	0.099	0.26	2.36

Table 6. Analysis of the raman spectra for ACF, ACF-O and ACF-S samples

Absorbent	~1,350 cm^{-1}		~1,600 cm^{-1}		~1,500 cm^{-1}		~1,200 cm^{-1}		1,580 cm^{-1}	
	M_{D1}	J_1	M_{D2}	J_2	M_{D3}	J_3	M_{D4}	J_4	G	J_t
ACF	15585.2	1.4	7267.2	0.69	1808.1	0.17	5309.3	0.50	10607.0	2.83
ACF-O	23421.6	4.1	9534.6	1.68	2607.4	0.46	4434.6	0.78	5678.6	7.28
ACF-S	25059.7	3.0	7499.2	0.91	32531.7	3.95	45581.1	5.54	8228.6	13.54

zation processes. This leads to the increase of the unsaturated carbon atoms in the corners and edges of the sample surface, which improves the adsorption capacity of Pb(II) ions.

1-5. XPS Analysis

The XPS wide-scan, C_{1s}, S_{2p} and N_{1s} spectra of ACF-O and ACF-S, sample are shown in Fig. 2. The two peaks around 163.74 eV and 170.22 eV assigned to the S_{2p} electron can be observed for XPS analysis of ACF-S sample, attributed to the sulfur containing functional groups in forms of -SH and SO_4^{2-} [50]. This confirms that thiol-functional groups from vulcanization treatment are successfully grafted onto the surfaces. The mass fraction of sulfur element increased from 0.17% to 6.51% after the thioglycolic-acid vulcanization treatment of ACF-O (Table 7). Two peaks of the C_{1s} spectra for the two samples can be observed at 284.75 and 288.95 eV (Fig. 2S(a) and (c)), attributed to the graphic carbon linkage (C-C) and carboxyl groups (O-C=O), respectively. The N_{1s} spectra

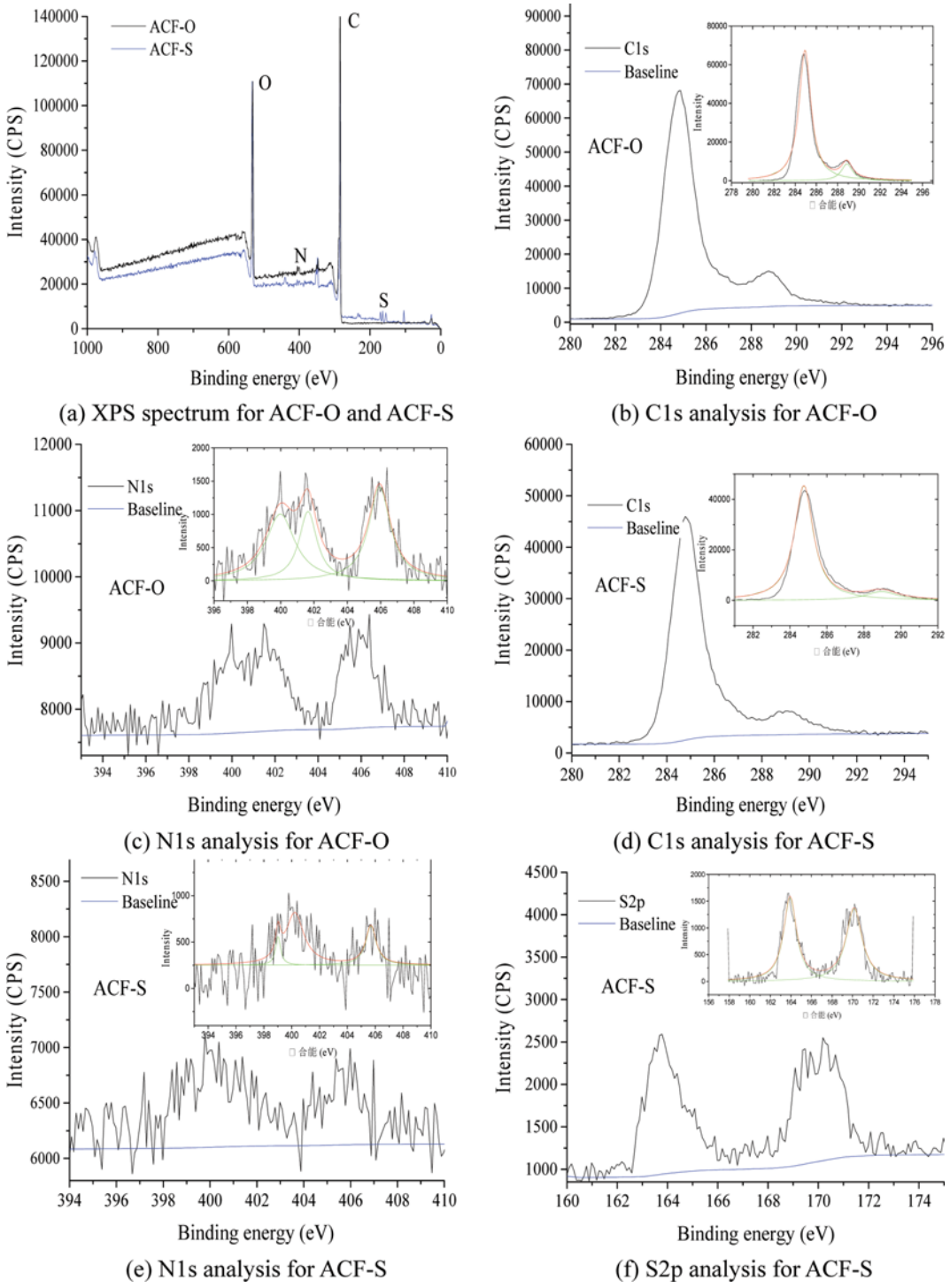

Fig. 2. XPS analysis for ACF-O and ACF-S samples.

Table 7. Distribution of S-, C- and N-contained functional groups and elemental weight percentage for ACF-O and ACF-S samples

Element	S			C			N			
Groups	-SH	SO_4^{2-}	Wt%	C-C	O-C(O)	Wt%	$-NO_2$	C-N	N-C(O)	Wt%
ACF-O	-	-	0.17	89.18%	10.82%	63.73	39.02%	37.29%	23.69%	3.12
ACF-S	48.13%	51.87%	6.51	88.48%	11.52%	60.04	27.78%	9.71%	62.51%	2.72

*Weight percentages of O were 32.98% and 30.73% for ACF-O and ACF-S samples

for the two samples exhibits three notable peaks around 399 eV for C-N group, 400 eV for N-C=O group and 405 eV for $-NO_2$ group. The atom percentage of O-C(O) and N-C(O) groups is distinctly increased for the ACF-S sample.

2. Performance of the Pb(II) Ions Adsorption by the Original and Modified ACF Samples

2-1. Effect of Contact Time

Effect of contact time on the adsorption capacity of Pb(II) ions by the ACF, ACF-O and ACF-S samples is shown in Fig. 3(a). The condition is pH, 5.5; concentration, 105 mg/L; and temperature, 25 °C. The adsorption capacity of the three samples was dramatically increased within 60 min, reaching 90% of their saturated adsorption capacity, and gradually reaching equilibrium stage. The fact is mainly ascribed to the sufficient available sites and strong electronegativity on the external absorbent surface in the initial stage of adsorption process. Moreover, the repulsive forces by adsorbate in solution or absorbent impose restrictions on the transfer resistance. The equilibrium state of the Pb(II) ions adsorption for ACF, ACF-O and ACF-S is located at around 90 min, achieving the adsorption capacity as 66.32 mg/g, 99.71 mg/g and 101.47 mg/g accordingly. The larger adsorption capacity of Pb(II) ions by ACF-O and ACF-S samples should be attributed to the sufficient active sites and strong electronegativity on the external surface.

2-2. Effect of Solvent Temperature

Effect of temperature on the adsorption capacity of Pb(II) ions by the ACF, ACF-O and ACF-S samples is shown in Fig. 3(b). The adsorption capacity of the three samples is enhanced to some extent by the increased solvent temperature due to the promotion of the

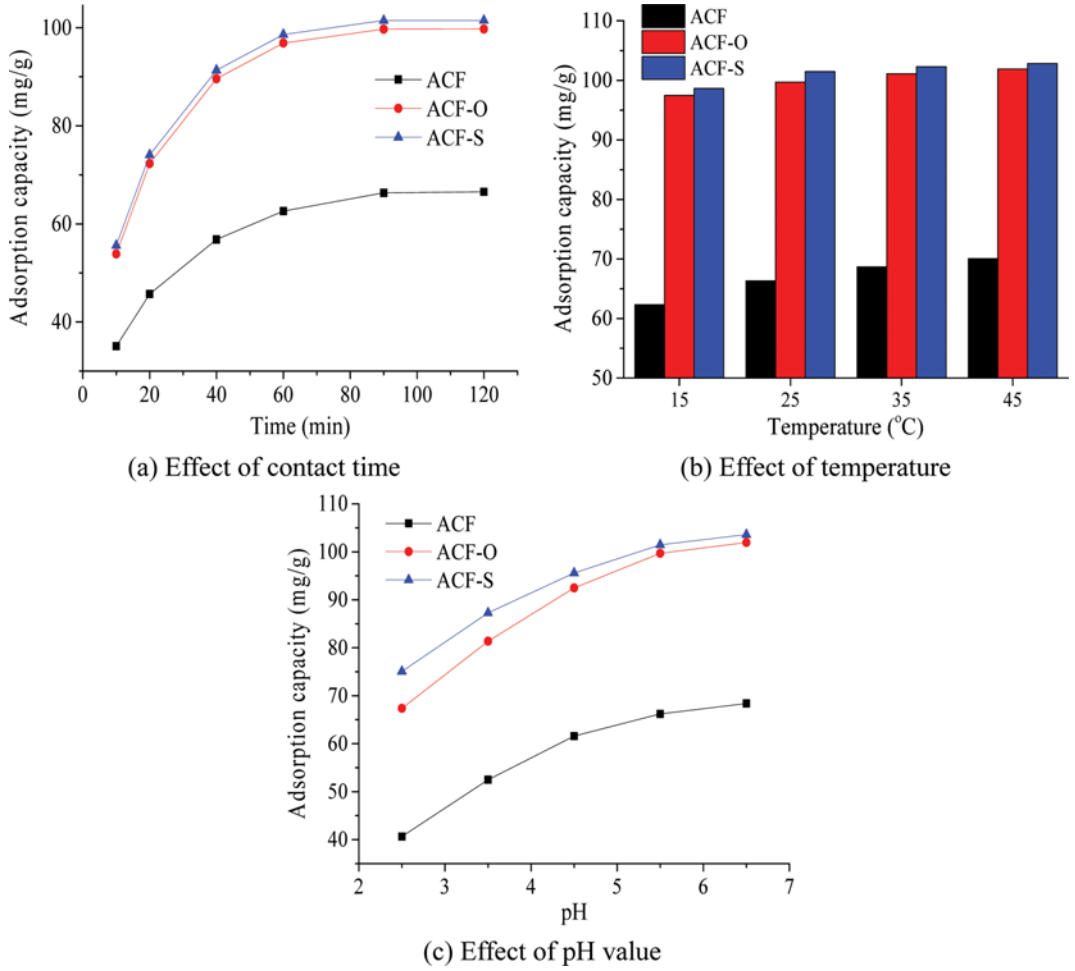

Fig. 3. The adsorption of Pb(II) ions by ACF, ACF-O and ACF-S samples.

Table 8. Thermodynamic analysis of Pb(II) ions Adsorption by the original and modified ACF samples

Absorbent	Temperature (K)	ΔG (J/mol)	ΔS (J/(mol·K))	ΔH (kJ/mol)
ACF	288	−5509.08	78.67	17.15
	298	−6295.74		
	308	−7082.41		
	318	−7869.07		
ACF-O	288	−6146.94	105.76	24.31
	298	−7204.56		
	308	−8262.19		
	318	−9319.81		
ACF-S	288	−6792.07	120.87	28.02
	298	−8000.76		
	308	−9209.45		
	318	−10418.1		

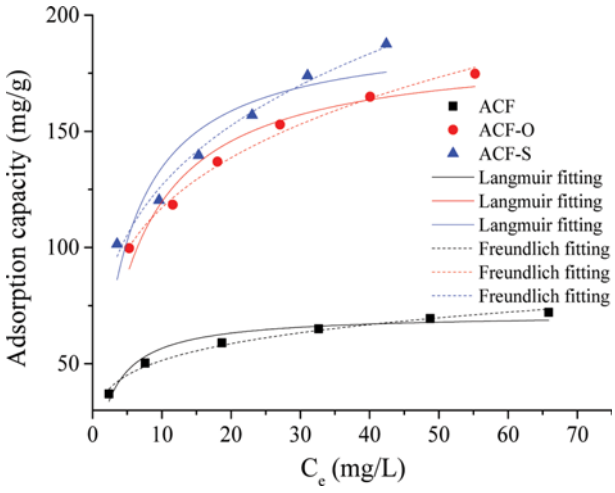

Fig. 4. The Langmuir and Freundlich isothermal models for the adsorption of Pb(II) by ACF, ACF-O and ACF-S samples.

mass transfer and diffusion rate of Pb(II) ions in the solution and on the adsorbent [51]. Thermodynamic analysis was employed for understanding the endothermic or exothermic property of the Pb(II) ions adsorption process by the original and modified ACF samples (Table 8). The adsorption enthalpy increased from 17.15 kJ/mol for ACF sample to 28.02 kJ/mol for ACF-S sample, indicating that the chemisorption during the the Pb(II) ions adsorption process by ACF-S is strongest among the three samples.

2-3. Effect of pH Value

Fig. 3(c) shows the effect of pH value (2.5-6.5) on the Pb(II) adsorption capacity of ACF, ACF-O and ACF-S samples. The adsorption capacity of Pb(II) ions by ACF sample is remarkably increased from 40.64 mg/g to 68.39 mg/g with the increased pH value, while that for ACF-O and ACF-S sample is increased from 67.37 mg/g to 101.94 mg/g and from 75.05 mg/g to 103.58 mg/g respectively. At low pH, H^+ is competitive with Pb(II) ions through occupying the available adsorption sites, leading to a decrease of adsorption capacity of Pb(II) ions. When the pH value exceeds the isoelectric point, Zeta potential of the original and modified ACF samples displays a negative charge, which is beneficial to removal of cation ions due to the electrostatic attraction. The carboxyl, hydroxyl and other functional groups on the surface of sample are easily disintegrated under the higher pH value, favoring the chemical adsorption of Pb(II) ions.

The possible status of Pb(II) ions in different pH value can be predicted by software Visual MINTEQ (Fig. 3S). When pH value is less than 6.0, Pb^{2+} ion is the major status for Pb(II) in the solution. $Pb(OH)^+$ and $Pb_3OH_4^{2+}$ ions become the dominant state for Pb(II) and easily precipitate simultaneously if the pH value is larger than 8 [52]. The pH value of solution in the experiments was set to be less than 6.5 to avoid the precipitation of Pb(II).

3. Isotherms of the Pb(II) Ions Adsorption by ACF, ACF-O and ACF-S Samples

Adsorption isotherm curve refers to the relationship curve between the two phases' concentration when solute molecules at certain temperatures are in the equilibrium state. The shape of an isotherm can reflect the possible patterns for the adsorption of Pb(II) ions on absorbents. Langmuir model and Freundlich model are employed to understand the adsorption process of Pb(II) ions by the original and modified ACF samples, giving the results in Fig. 4 and Table 9. The maximum adsorption capacity of ACF, ACF-O and ACF-S samples at 25 °C is determined by Langmuir method as 75.24 mg/g, 193.42 mg/g and 209.21 mg/g respectively. It confirms that the adsorption capacity of ACF sample can be substantially improved by the nitric-acid oxidation and thioglycolic-acid vulcanization which can be attributed to the improvement of the pore structure and surface chemistry properties. While ACF-S presented an adsorption capacity higher than that of ACF-O indicating that the existence of sulfur containing functional groups and ester groups may make important contributions to Pb(II) adsorp-

Table 9. The parameters calculated from Langmuir and Freundlich isothermal models for ACF, ACF-O and ACF-S samples

Model	Parameters	ACF		ACF-O		ACF-S	
		15 °C	25 °C	15 °C	25 °C	15 °C	25 °C
Langmuir method	q_0 (mg/g)	72.67	75.24	191.94	193.42	207.04	209.21
	b (L/mg)	0.1528	0.2556	0.1167	0.1513	0.1193	0.1611
	r^2	0.8351	0.9332	0.9723	0.9391	0.9391	0.8732
Freundlich method	n	4.06	4.38	3.78	4.10	3.38	3.75
	k_f (mg/g)	24.72	27.83	58.51	66.85	56.35	68.66
	r^2	0.9821	0.9854	0.9737	0.9896	0.9967	0.9836

Table 10. Adsorption capacity of Pb(II) ions by the modified adsorbents in literature determined by Langmuir model

Precursors	Modification methods	q_0 (mg/g)	Conditions
Carbon nanotube sheets [46]	HNO_3	117.65	7.0
Nanotube [47]	-	97.08	5.0
Mesoporous carbon [48]	HNO_3	94	5.0
SBA-15 [49]	-SH	173	6.0
Coconut-based activated carbon [50]	H_2O_2	28.46	4.3-4.7
	HNO_3	40.12	3.2-3.6
	-	75.24	5.5
Sisal ACF [present work]	HNO_3	193.42	5.5
	HNO_3 and -SH	209.21	5.5

tion. The value for some other modified absorbents reported in literature is listed in Table 10, exhibiting the outstanding performance of Pb(II)adsorption capacity by the modified ACF samples in this study.

The Freundlich model fits the experimental data better than that of Langmuir model, indicating the multilayer adsorption is dominated during the Pb(II) ions adsorption process. The parameter of n from the Freundlich model is between 2 and 10 for the ACF-O and ACF-S samples, demonstrating that the Pb(II) ions adsorption process by the modified ACF samples is easy to proceed.

4. Adsorption Kinetics for Pb(II) Removal by the ACF Samples

First-order, second-order and intra-particle diffusion kinetic model are widely used for describing the adsorption process of heavy metals by absorbents in the literature [53-55]. However, the inherent mechanism involving the liquid film mass transfer or intra-particle diffusion is always ignored in the models. The homogeneous surface diffusion model (HSDM) considering the intra-particle diffusion and liquid mass transfer is employed for describing the Pb(II) ions adsorption process by the original and modified ACF samples. The assumptions for HSDM are listed as: a) the sur-

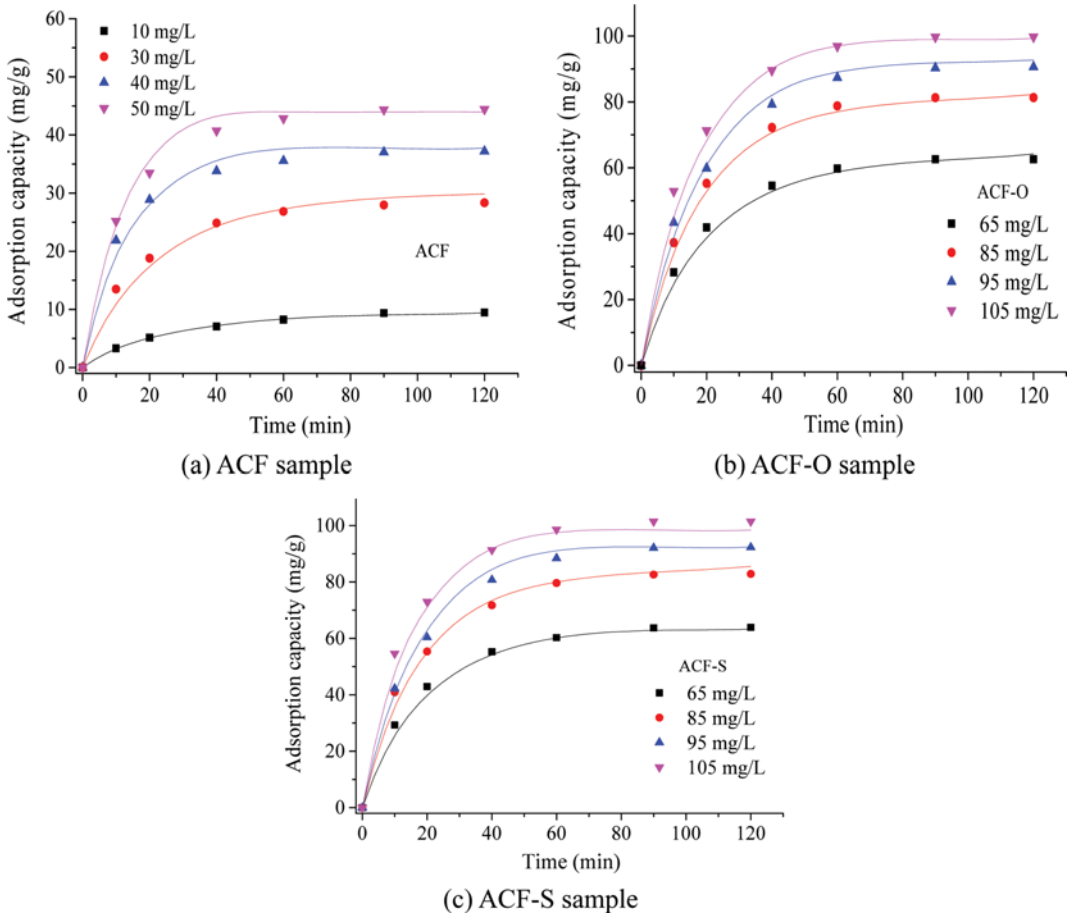

Fig. 5. The comparison between the experimental data and predictions from the HSDM model.

face of the adsorbent is homogeneous and absorbent can be equivalent to spherical particle; b) Intra-particle diffusion is controlled by surface diffusion; c) the liquid film mass transfer is denoted by the linear driving force; d) the mass transfer on the solid-liquid interface is continuous; e) equilibrium state of the adsorption process on solid-liquid interface is instantaneous achieved; and f) adsorption system is operated under constant temperature [56].

According to the second Fick Law, the adsorption rate of Pb(II) ions by the samples can be expressed as:

$$\frac{\partial q}{\partial t}=\frac{1}{r^2}\frac{\partial}{\partial r}\left(r^2 D_s\frac{\partial q}{\partial r}\right) \tag{7}$$

where q is the adsorption capacity at radius r and time t, mg/g; D_s is the surface diffusion coefficient, m^2/s.

The driving force is described as:

$$\rho\frac{\partial \bar{q}}{\partial t}=k_f a_p(C-C_s) \tag{8}$$

where k_f is the liquid-film coefficient of mass transfer, m/s; ρ is the apparent density, kg/m^3; $\bar{q}$ is the average adsorption capacity in the granule at time t, mg/g; C_s is the concentration on the surface of liquid-solid at time t, mg/L; a_p is the ratio of the surface area and volume, m^{-1}.

The boundary conditions are:

$$D_s a_p\left.\frac{\partial q}{\partial r}\right|_{r=r_p}=\frac{\partial \bar{q}}{\partial t}=\frac{k_f}{\rho}a_p(C-C_s) \tag{9}$$

$$\left.\frac{\partial q}{\partial r}\right|_{r=0}=0 \tag{10}$$

The initial condition is:

$$q|_{t=0}=0 \tag{11}$$

The relationship between $\bar{q}$ and q can be calculated as:

$$\bar{q}=\frac{3}{r_p^3}\int_0^{r_p} q r^2 dr \tag{12}$$

The correlation coefficient is estimated as:

$$rr^2=1-\frac{\Sigma(C-\widehat{C})^2}{\Sigma(C-\bar{C})^2} \tag{13}$$

The *Biot* number is determined as [57]:

$$Bi=\frac{k_f r_p C_0}{D_s \rho q_e} \tag{14}$$

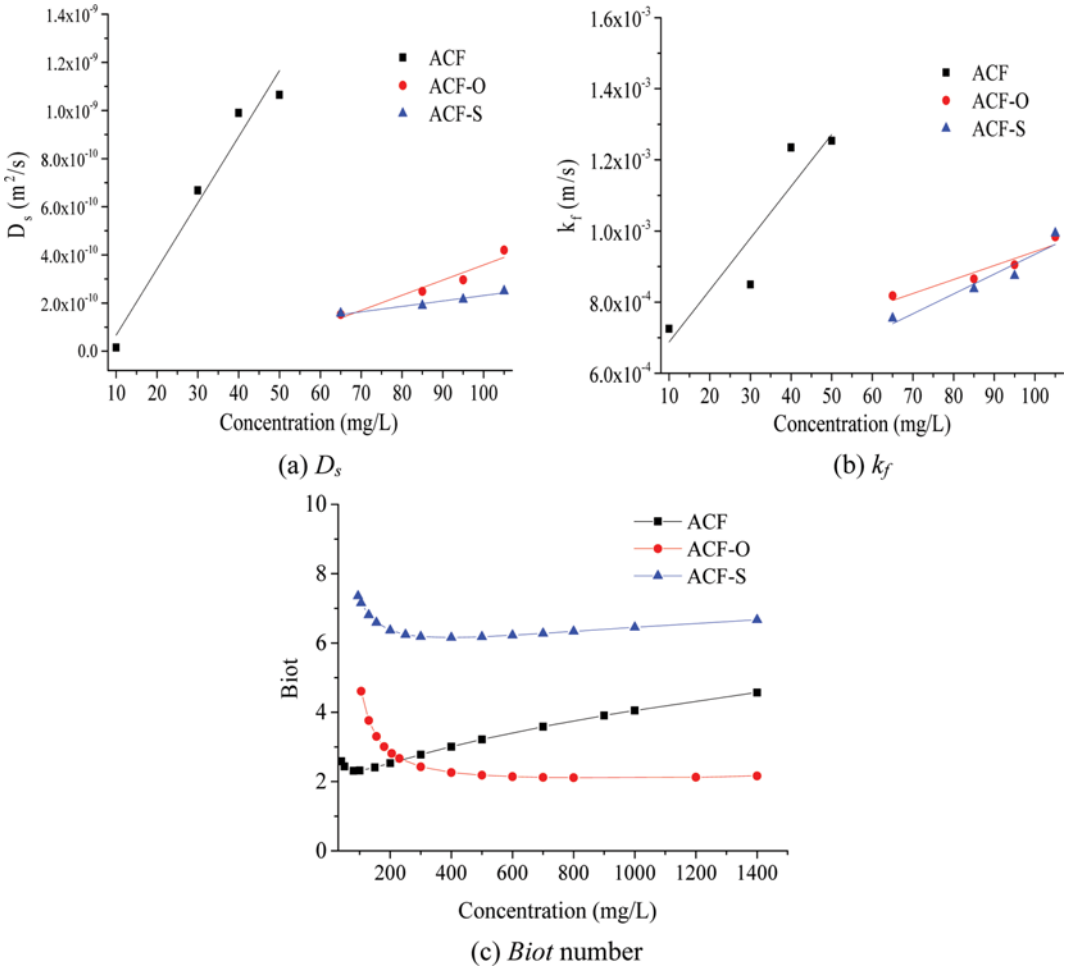

Fig. 6. Distribution of the calculated diffusion coefficient (D_s), mass transfer parameter (k_f) and *Biot* number against the initial Pb(II) concentration for the ACF, ACF-O and ACF-S samples.

Eqs. (9)-(14) can be solved by the software Matlab. The D_s and k_f can be calculated while the correlation coefficient reaches the maximum value. It can be found that the prediction from HSDM fits the experiment data very well (Fig. 5). The surface diffusion coefficient (D_s) is linearly increased with the initial concentration of Pb(II) ions (Fig. 6(a)), giving the correlation coefficient as 0.9631, 0.9375 and 0.9633 for ACF, ACF-O and ACF-S, respectively. The liquid-film coefficient of mass transfer (k_f) is also linearly increased with the initial concentration of Pb(II) ions (Fig. 6(b)), giving the correlation coefficient as 0.8589, 0.9141 and 0.9175 accordingly. This indicates that the ability of adsorbate imigrating from bulk solution towards the adsorbent can be substantially enhanced with the increase of Pb(II) ions initial concentration.

The predicted magnitude of *Biot* number calculated through Eq. (14) is first decreased with the initial Pb(II) concentration and then increased to different extent for the ACF, ACF-O and ACF-S samples. If the *Biot* number is less than 1, the adsorption process is limited by film mass transfer. While if the *Biot* number is between 1 and 100, the surface diffusion and film mass transfer both play an important role in the adsorption process. Otherwise, the adsorption process is prominently controlled by the surface diffusion [58]. The *Biot* numbers of ACF, ACF-O and ACF-S samples are all between 1 and 100 (Fig. 6(c)), confirming that the adsorption process of Pb(II) ions by the samples is limited by both the surface diffusion and film mass transfer. The *Biot* number for ACF-S sample is higher than that of ACF and ACF-O under different Pb(II) ions initial concentrations, suggesting that adsorption process of ACF-S is largely limited by the surface diffusion over that of the other two samples.

CONCLUSIONS

The integrated technology of microwave-assisted nitric-acid oxidation and thioglycolic-acid vulcanization was developed and applied for the modification of sisal-based activated carbonaceous fiber (ACF). The optimum condition for the microwave-assisted nitric-acid oxidation process was determined regarding the maximum adsorption capacity of Pb(II) ions: concentration of nitric acid as 9.5 mol/L, modification time as 15 min, modification temperature as 150 °C and microwave power as 800 W. The physico-chemical properties of ACF sample were greatly improved through the modification process, such as the micro-pore distribution, the content of oxygen-contained acidic/polar functional groups and thiol-functional groups on surface. The maximum adsorption capacity of Pb(II) by the modified ACF samples was substantially increased to 200 mg/g (193.42 mg/g for ACF-O and 209.21 mg/g for ACF-S), compared to that of 75.24 mg/g for the original ACF sample. The adsorption process of Pb(II) ions by the original and modified ACF samples can be well fitted by Freundlich isothermal model. The *Biot* number calculated from the homogeneous surface diffusion model (HSDM) was between 1 and 100 for the original and modified ACF samples, suggesting that the adsorption process of Pb(II) ions is limited by both the surface diffusion and film mass transfer.

ACKNOWLEDGEMENTS

The authors greatly acknowledge the funding support from the projects supported by National Natural Science Foundation of China (Grant No. 51476034), National Basic Research Program of China (973 Program) Natural Science Foundation of Jiangsu Province, China (Grant No. BK20141451).

SUPPORTING INFORMATION

Additional information as noted in the text. This information is available via the Internet at http://www.springer.com/chemistry/journal/11814.

REFERENCES

1. B. M. Babić, S. K. Milonjić and M. J. Polovina, *Carbon*, **40**(7), 1109 (2002).
2. N. H. Phan, S. Rio, C. Faur, L. Le Coq, P. Le Cloirec and T. H. Nguyen, *Carbon*, **44**(12), 2569 (2006).
3. Q. S. Liu, T. Zheng, P. Wang, J. P. Jiang and N. Li, *Chem. Eng. J.*, **157**(2), 348 (2010).
4. J.-T. Chung, K.-J. Hwang, W.-G. Shim, C. Kim, J.-Y. Park, D.-Y. Choi and J.-W. Lee, *Mater. Lett.*, **93**, 401 (2013).
5. C. Pelekani and V. L. Snoeyink, *Carbon*, **38**(10), 1423 (2000).
6. H. Tamai, T. Yoshida, M. Sasaki and H. Yasuda, *Carbon*, **37**(6), 983 (1999).
7. K. C. Kang, S. S. Kim, J. W. Choi and S. H. Kwon, *J. Ind. Eng. Chem.*, **14**(1), 131 (2008).
8. G. H. Xiu and P. Li, *Carbon*, **38**(7), 975 (2000).
9. D. Y. Tang, Z. Zheng, K. Lin, J. F. Luan and J. B. Zhang, *J. Hazard. Mater.*, **143**(1), 49 (2007).
10. L. Zhou, *Renew. Sust. Energy Rev.*, **9**(4), 395 (2005).
11. J. P. Chen, S. Wu and K.-H. Chong, *Carbon*, **41**(10), 1979 (2003).
12. V. K. Gupta, A. Nayak and S. Agarwal, *Environ. Eng. Res.*, **20**(1), 1 (2015).
13. T. A. Saleh and V. K. Gupta, *Adv. Colloid Interface*, **211**, 93 (2014).
14. V. K. Gupta and T. A. Saleh, *Environ. Sci. Pollut. R.*, **20**(5), 2828 (2013).
15. V. K. Gupta, R. Kumar, A. Nayak, T. A. Saleh and M. A. Barakat, *Adv. Colloid Interface Sci.*, **193-194**, 24 (2013).
16. S. Karthikeyan, V. K. Gupta, R. Boopathy, A. Titus and G. Sekaran, *J. Mol. Liq.*, **173**, 153 (2012).
17. V. K. Gupta, A. Mittal, D. Jhare and J. Mittal, *RSC Adv.*, **2**(22), 8381 (2012).
18. A. K. Jain, V. K. Gupta, A. Bhatnagar and Suhas, *Sep. Sci. Technol.*, **38**(2), 463 (2003).
19. X. Ge, X. Ma, Z. Wu, X. Xiao and Y. Yan, *Res. Chem. Intermediat.*, **41**(10), 7327 (2014).
20. A. Lisovskii, G. E. Shter, R. Semiat and C. Aharoni, *Carbon*, **35**(10), 1645 (1997).
21. W. Shen, Z. Li and Y. Liu, *R. Pat. Chem. Eng.*, **1**(1), 27 (2010).
22. S. Yao, J. Zhang, D. Shen, R. Xiao, S. Gu, M. Zhao and J. Liang, *J. Colloid Interface Sci.*, **463**, 118 (2016).
23. I. L. Lagadic, M. K. Mitchell and B. D. Payne, *Environ. Sci. Technol.*, **35**(5), 984 (2001).
24. X. Xue and F. Li, *Micropor. Mesopor. Mater.*, **116**(1-3), 116 (2008).
25. T. T. X. Dong, K. J. Zhao, W. Z. Huang, K. W. Leung and K. W. K. Tsim, *Phytother. Res.*, **19**(8), 684 (2005).

26. S. Suresh, V. C. Srivastava and I. M. Mishra, *Theor. Found. Chem. Eng.*, **47**(3), 284 (2013).
27. J. A. Menendez, M. J. Illán-Gómez, Y. Leon and R. Radovic, *Carbon*, **33**(11), 1655 (1995).
28. P. Chingombe, B. Saha and R. J. Wakeman, *Carbon*, **43**(15), 3132 (2005).
29. T. C. Chandra, M. M. Mirna, J. Sunarso, Y. Sudaryanto and S. Ismadji, *J. Taiwan Inst. Chem. E.*, **40**(4), 457 (2009).
30. R. Hoseinzadeh Hesas, A. Arami-Niya, W. M. A. Wan Daud and J. N. Sahu, *J. Anal. Appl. Pyrol.*, **104**, 176 (2013).
31. A. Sadezky, H. Muckenhuber, H. Grothe, R. Niessner and U. Pöschl, *Carbon*, **43**(8), 1731 (2005).
32. H. Wang, A. Zhou, F. Peng, H. Yu and J. Yang, *J. Colloid Interface Sci.*, **316**(2), 277 (2007).
33. J.-L. Gong, Y.-L. Zhang, Y. Jiang, G.-M. Zeng, Z.-H. Cui, K. Liu, C.-H. Deng, Q.-Y. Niu, J.-H. Deng and S.-Y. Huan, *Appl. Surf. Sci.*, **330**, 148 (2015).
34. C. Parat, J. Y. Cornu, A. Schneider, L. Authier, V. Sapin-Didier, L. Denaix and M. Potin-Gautier, *Anal. Chim. Acta*, **648**(2), 157 (2009).
35. H. Parshotam, G. Gericke, J. C. Ngila and S. Mishra, *Water SA*, **42**(1), 171 (2016).
36. M. Shahid, C. Dumat, M. Aslam and E. Pinelli, *Chem. Spec. Bioavailab.*, **24**(4), 248 (2012).
37. W. T. Tan, S. T. Ooi and C. K. Lee, *Environ. Technol.*, **14**(3), 277 (1993).
38. C. P. Dwivedi, J. N. Sahu and C. R. Mohanty, *J. Hazard. Mater.*, **156**(1), 596 (2008).
39. H. Chen, J. Zhao, J. Wu and G. Dai, *J. Hazard. Mater.*, **192**(1), 246 (2011).
40. M. I. Bautista-Toledo, J. Rivera-Utrilla and R. Ocampo-Pérez, *Carbon*, **73**, 338 (2014).
41. S. Shrestha, G. Son, S. H. Lee and T. G. Lee, *Chemosphere*, **92**(8), 1053 (2013).
42. C. Theivarasu and S. Mylsamy, *Int. J. Eng. Sci. Technol.*, **2**(11), 6284 (2010).
43. E. A. Oliveira, S. F. Montanher, A. D. Andrade, J. A. Nóbrega and M. C. Rollemberg, *Process Biochem.*, **40**(11), 3485 (2005).
44. A. K. Kercher and D. C. Nagle, *Carbon*, **41**(1), 15 (2003).
45. C. Xu, N. Tsubouchi, H. Hashimoto and Y. Ohtsuka, *Fuel*, **84**(14-15), 1957 (2005).
46. Y. Chen, Y. Zhu, Z. Wang, Y. Li, L. Wang, L. Ding, X. Gao, Y. Ma and Y. Guo, *Adv. Colloid Interface Sci.*, **163**(1), 39 (2011).
47. C. Chen, X. Li, Z. Tong, Y. Li and M. Li, *Appl. Surf. Sci.*, **315**, 203 (2014).
48. Y.-H. Li, S. Wang, Z. Luan, J. Ding, C. Xu and D. Wu, *Carbon*, **41**(5), 1057 (2003).
49. C. Sheng, *Fuel*, **86**(15), 2316 (2007).
50. L. Chai, Q. Li, Y. Zhu, Z. Zhang, Q. Wang, Y. Wang and Z. Yang, *Bioresour. Technol.*, **101**(15), 6269 (2010).
51. I. A. A. Hamza, B. S. Martincigh, J. C. Ngila and V. O. Nyamori, *Phys. Chem. Earth, Parts A/B/C*, **66**, 157 (2013).
52. J. Huang, M. Ye, Y. Qu, L. Chu, R. Chen, Q. He and D. Xu, *J. Colloid Interface Sci.*, **385**(1), 137 (2012).
53. R. Karthik and S. Meenakshi, *Chem. Eng. J.*, **263**, 168 (2015).
54. M. K. Sahu, S. Mandal, S. S. Dash, P. Badhai and R. K. Patel, *J. Environ. Chem. Eng.*, **1**(4), 1315 (2013).
55. S. Chakravarty, A. Mohanty, T. N. Sudha, A. K. Upadhyay, J. Konar, J. K. Sircar, A. Madhukar and K. K. Gupta, *J. Hazard. Mater.*, **173**(1-3), 502 (2010).
56. R. M. C. Viegas, M. Campinas, H. Costa and M. J. Rosa, *Adsorption*, **20**(5-6), 737 (2014).
57. K. Satoh, H. J. Fan, H. Hattori, K. Tajima and E. Furuya, *J. Hazard. Mater.*, **155**(3), 397 (2008).
58. S. Baup, C. Jaffre, D. Wolbert and A. Laplanche, *Adsorption*, **6**(3), 219 (2000).

Supporting Information

Pb(II) ion adsorption by biomass-based carbonaceous fiber modified by the integrated oxidation and vulcanization

Xiaoxiang Jiang* **and Dekui Shen****,†

*Engineering Laboratory of Energy System Process Conversion & Emission Control Technology of Jiangsu Province, School of Energy and Mechanical Engineering, Nanjing Normal University, Nanjing 210042, P. R. China
**Key Laboratory of Energy Thermal Conversion and Control of Ministry of Education, Southeast University, Nanjing 210096, P. R. China
(*Received 16 May 2016 • accepted 12 June 2017*)

EXPERIMENTS

Orthogonal Test:

Two significant parameters of K_{ij} and R_i are analyzed in a range analysis. K_{ij} is defined as the sum of the experimental indexes of all levels of factor i. The k_{ij} is the mean value of K_{ij} for estimating optimal level. The optimal level of each factor is the largest value of K_{ij}. R_i is the range between the maximum and minimum value of k_{ij} and the largest R_i implies the greatest importance of the factor i. The calculation of factor A is shown in Eq. (S1)-(S5):

$$K_{A1}=Z_{A1}+Z_{A2}+Z_{A3}+Z_{A4} \quad \text{(S1)}$$

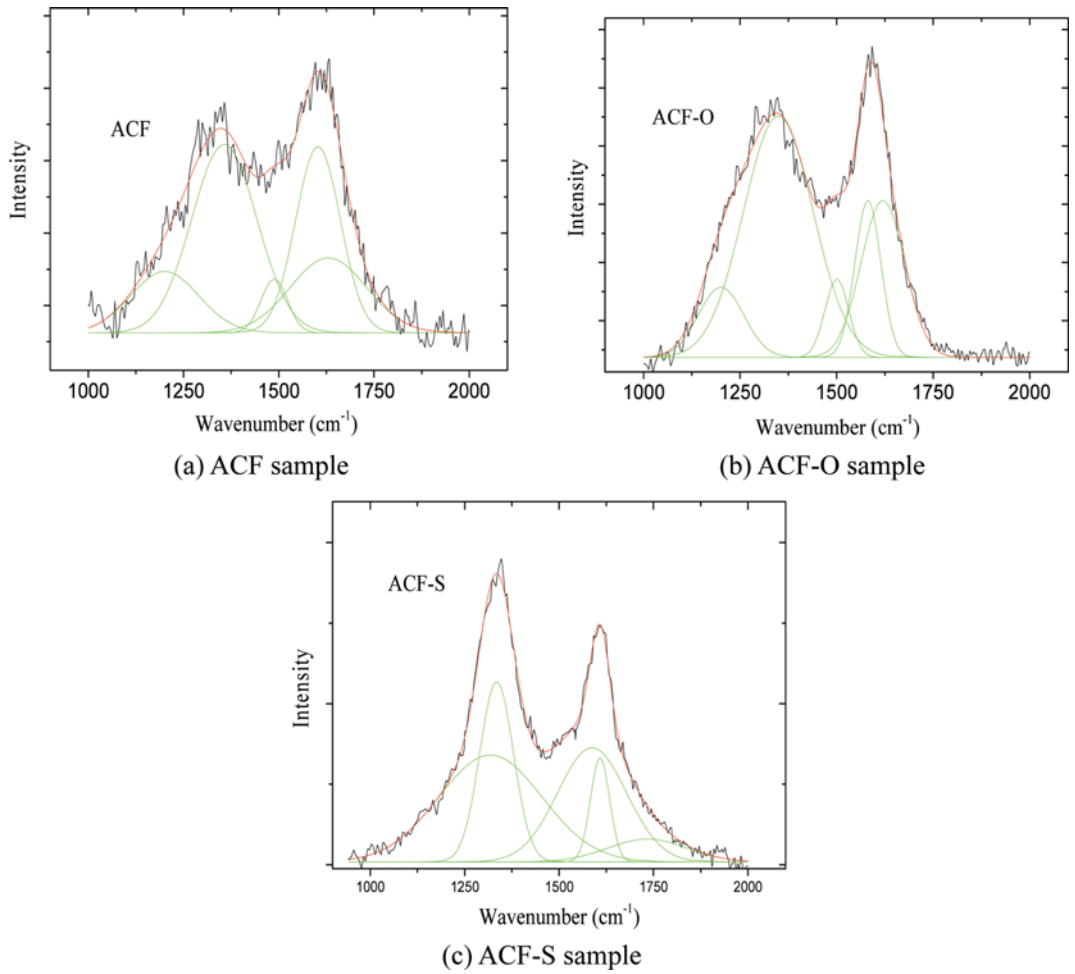

Fig. S1. Gaussian fitting for the G and D_i band on Raman spectrum of ACF, ACF-O and ACF-S samples.

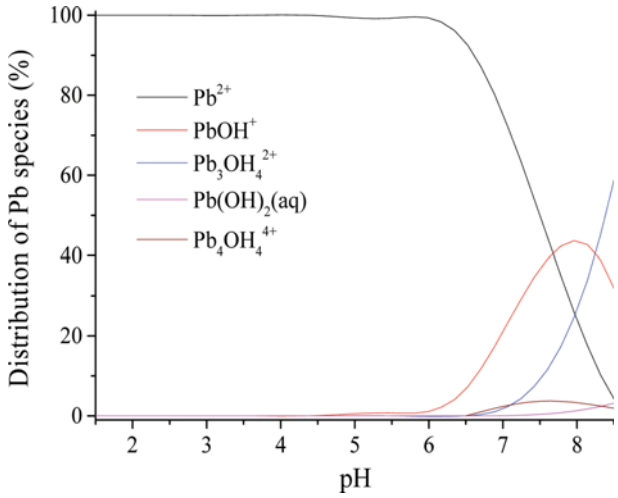

Fig. S2. Effect of pH value on Pb(II) ions species determined by Visual MINTEQ (the concentration of Pb ions is set as 100 mg/L).

$$K_{A2}=Z_{A5}+Z_{A6}+Z_{A7}+Z_{A8} \quad (S2)$$

$$K_{A3}=Z_{A9}+Z_{A10}+Z_{A11}+Z_{A12} \quad (S3)$$

$$k_{A1}=K_{A1}/4;\ k_{A2}=K_{A2}/4;\ k_{A3}=K_{A3}/4;\ k_{A4}=K_{A4}/4 \quad (S4)$$

$$R_A=\max(k_{Aj})-\min(k_{Aj}) \quad (S5)$$

where Z_{Aj} is the value of adsorption capacity for the experiment j.

The optimal condition can be obtained by the range analysis, but the method cannot determine whether the variation of data is caused by experimental factors or errors. Due to the restriction of range analysis, the variance analysis is necessary to be employed for confirming the data analysis.

The sum of square deviation for each factor (SS_i) is shown in Eq. (S6)

$$SS_i=\frac{1}{4}\sum_{j=1}^{4}K_{ij}^2-\left(\sum_{j=1}^{16}Z_{ij}\right)^2/16 \quad (S6)$$

In the similar way, the sum of square deviation of error (SS_e) is shown in Eq. (S7)

$$SS_e=\frac{1}{4}\sum_{j=1}^{4}K_{ej}^2-\left(\sum_{j=1}^{16}Z_{ij}\right)^2/16 \quad (S7)$$

The variance of each factor and error can be expressed as Eq. (S8)-(S10)

$$MS_i=SS_i/df=SS_i/3\ (i=A, B, C, D) \quad (S8)$$

$$MS_e=SS_i/df=SS_e/3 \quad (S9)$$

Therefore, the *F* value for each factor *i* is determined as:

$$F_i=MS_i/MS_e \quad (S10)$$

$F_a(f_i, f_e)$ is defined as the critical value of F-test. If F_i is larger than $F_{0.01}$, the effect of factor is highly significant. If the F_i ratio is between $F_{0.01}$ and $F_{0.05}$, the factor effect is significant. Otherwise, the effect of factor is not significant.

Raman Analysis:

The parameters of J and Cs in Eq. (S11) and Eq. (S12) is employed to characterize the chaos and graphite crystal size. M_{Di} and M_G are the peak area ratio of D_i band and G band, calculated by Gaussian peak fitting function.

$$J_i=M_{Di}/M_G\ J_t=M_{Dt}/M_G \quad (S11)$$

$$Cs=44/J_t \quad (S12)$$